Monitoring the Formation Kinetics of a Bicontinuous Microemulsion

Delphine Herrera, Thibaud Chevalier, Didier Frot, Loïc Barré, Audrey Drelich, Isabelle Pezron, Christine Dalmazzone

Monitoring the formation kinetics of a bicontinuous microemulsion.

Delphine Herrera[1], Thibaud Chevalier[1], Didier Frot[1], Loïc Barré[1], Audrey Drelich[2], Isabelle Pezron[2], Christine Dalmazzone[1].

[1] *IFP Energies nouvelles, 1 et 4 avenue de Bois-Préau, 92852 Rueil-Malmaison Cedex – France*

[2] *Université de technologie de Compiègne, ESCOM, TIMR (Integrated Transformations of Renewable Matter), Centre de recherche Royallieu - CS60319 - 60203 Compiègne Cedex, France*

Corresponding author: Christine Dalmazzone

E-mail address of the corresponding author: christine.dalmazzone@ifpen.fr

Keywords : Microemulsions, Bicontinuous, Formation, Quantification, Structure, DLS, NMR, Micro-CT, SAXS

Abstract

Hypotheses

The performance of bicontinuous microemulsions is usually assessed on the characteristics of the middle phase at equilibrium. However, applied to Enhanced Oil Recovery, such an evaluation would not be representative of the structure and composition of fluids in reservoir rocks. Studies on the properties of non-equilibrated microemulsions are still needed to better understand the formation of such complex systems, in particular to optimize input parameters of process simulation tools.

Experiments

For this purpose, we monitored the formation of a microemulsion from contact with the oil to equilibrium when no mixing or convection is provided. Non-destructive methods such as Nuclear Magnetic Resonance, Micro-Computed Tomography, Dynamic Light Scattering and Small Angle X-ray scattering were used to extract the compositions, phase thicknesses, dynamics and structures of the system over time.

Finding

We found that the system gets structured into several layers over time that include the transient presence of an oriented semi-crystalline phase. The growth of the bicontinuous middle phase results from a progressive reorganization of the liquid crystal. The compositional and structural gradients, observed along the sample height, are correlated and linked to the corresponding structures of the phase diagram of the quaternary system. Equilibrium is reached after the total transfer of the liquid crystal into the bicontinuous phase.

Graphical abstract

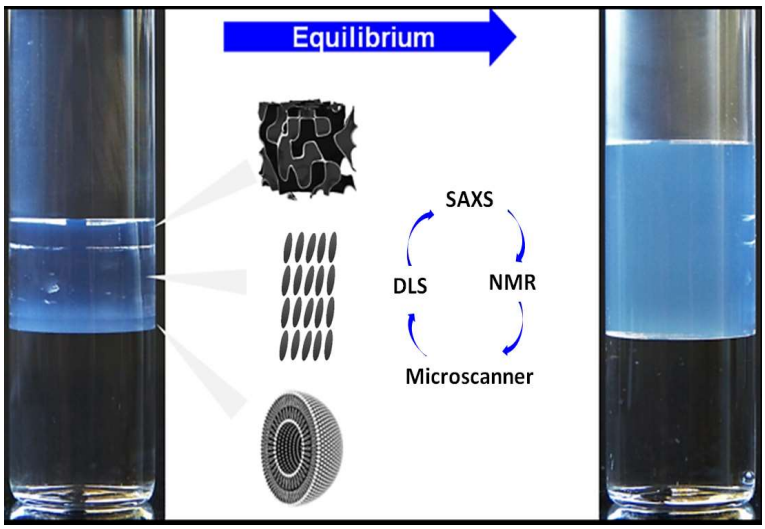

1. Introduction

Since their discovery in 1959 [1], microemulsions have been intensively studied due to their remarkable properties such as low viscosity, isotropic and thermodynamically stable phases as well as ultralow interfacial tensions between oil and water [2][3]. They are used today in a wide variety of applications in all fields of chemistry such as cosmetic, chemical, pharmaceutical, food and oil industries mainly for their high oil solubilization performance. Particularly in Enhanced Oil Recovery (EOR), the use of microemulsions appears to be a good alternative to extract the crude that is trapped by capillary forces into the porous reservoir rock. When injecting an optimal surfactant-rich formulation, a microemulsion should form after contact with the crude. When anionic surfactants are used, a co-surfactant (alcohol type) is often added to the formulation to enhance the interfacial film fluidity and allow the formation of the microemulsion. In most studies, the optimal formulation is determined according to the performances of the microemulsion at equilibrium. However, this evaluation may not be representative of the behavior of fluids in situ in the reservoir [4]. In a real porous rock, two situations may occur: either the pores are interconnected, or they are dead-end pores. In the first case, convection processes ensure a natural mixing of fluids in situ leading to a quasi-instantaneous formation of the microemulsion. In the second case, no source of mixing is provided. Recently, Broens et al. [5] studied such micro-emulsification in a microfluidics set up by modeling the dead ends pores of a reservoir. In this configuration, they confirmed that the formation of the microemulsion is only controlled by diffusion phenomena that take place in the pore space. By monitoring the penetration front of the microemulsion under fluorescence microscopy, they indicated that the kinetics of micro-emulsification obeys Fick's law. However, if matter exchanges are limited by diffusion, one can wonder if the bicontinuous microemulsion is properly formed in situ. In 2019, Unsal et al. [6] investigated the micro-emulsification of a bicontinuous microemulsion under flow in a model porous rock using quantitative X-ray micro-tomography. They directly proved the presence of local gradients of composition in the vicinity of the dead-end pores in the porous rock. However, current methodologies and analytical instruments are limited in accessing local properties and structure of fluids in these complex regions. To some extent, these data would be particularly useful for optimizing oil recovery processes and better understanding plugging issues during flow. We thus propose to work on the mechanisms of formation of a bicontinuous microemulsion, in bulk and under static conditions, when only diffusion processes are present. The challenge is to have access to local and quantitative information over time without affecting the diffusion phenomena occurring in situ in the system. In particular, analytical methods that allow quantitative kinetic studies of the formation of microemulsions are scarce. The usual chemical techniques such as Karl-Fischer or Hyamine titrations [7,8] as well as gas chromatography [9,10] are destructive and relatively time-consuming for kinetic perspectives. In addition, these methods do not allow simultaneous and local quantification of a multi-component system. In this objective, we benefited from the complementarity of Low-Field Nuclear Magnetic Resonance (NMR), X-Ray Micro-Computed Tomography (Micro-CT), Dynamic Light Scattering (DLS) and Small Angle X-Ray Scattering (SAXS) to monitor the formation of a bicontinuous microemulsion from phases contact to equilibrium. The studied microemulsion is a quaternary system containing toluene/NaCl brine/butan-1-ol/Sodium dodecylsulfate [11] at optimal formulation. The in-house NMR method was developed to obtain composition profiles of oil, brine and co-surfactant along the sample height [12]. Micro-CT enabled precise acquisitions of phase thicknesses and volume fraction of brine in the sample. Finally, we correlated the compositional information collected from these techniques with SAXS and DLS measurements which provided respectively local and dynamic information on the structure. The methods implemented in this work are non-destructive and the measurements are fast enough to allow kinetic monitoring.

2. Experiments

2.1. Products

The surfactant, Sodium dodecylsulfate, (dry weight > 98.5%, water <1.5%) was supplied by Alfa Aesar and was used without further purification. Toluene was from VWR (AnalaR Normapur), butan-1-ol and

sodium chloride NaCl were from Merck (grade analysis). Milli-Q water was used (HX7000 from Merck, Resistivity 10-15 MΩ.cm; Conductivity < 0.2 µS/cm at 25°C).

2.2. Microemulsions systems

The Winsor III system studied is made of NaCl brine, Sodium dodecylsulfate "SDS" (surfactant), butan-1-ol (co-surfactant) as aqueous phase and toluene as oil phase. Compositions were calculated to satisfy a water-to-oil volume ratio WOR = 1; co-surfactant = 5.5 % v/v. of the total system; co-surfactant/Surfactant weight ratio = 2. More details on the formulation steps can be found in Supplementary Material Part I. Experiments were carried out on a microemulsion at optimal formulation (Hydrophilic Lipophilic Deviation = 0)[13] corresponding to an aqueous phase salinity of 54 g/L of NaCl. The microemulsion was directly formulated in 1.5 mm-diameter quartz capillaries for SAXS (50 µL) and in 1.8 cm diameter glass tubes for NMR (3 mL), Micro-CT and DLS (10 mL).

2.3. Kinetics studies

Kinetic studies were performed by NMR, Micro-CT and DLS. SAXS was used punctually to characterize the structures encountered during the process. We first independently formulated the aqueous phase of the microemulsion as described above. Toluene was added at a controlled speed of 126.8 mL/h via an automatic syringe pump on the aqueous phase without any stirring or mixing. After Toluene addition, the vials were sealed with caps and Teflon rubber to avoid evaporation. During NMR experiments, the samples were inserted into the probe and the temperature was set at 30°C by temperature-controlled air stream. While in the DLS, Micro-CT and SAXS tests, the experiments were carried out at room temperature (20°C) as no temperature control device is present on these experimental setups. To verify if any change of structure occurs at a warmer temperature (between 20 and 30°C), the equilibrated microemulsion was left to rest 1 day in an oven at 40°C. We did not notice any change in the thicknesses of the triphasic system nor any change in the aspect of the intermediate phase. Thus we assume that the temperature difference between the setups environment does not significantly affect the structure and composition of each phase in the sample which are still comparable. The measurements along the tube height were performed under completely static conditions until equilibrium was reached. Once equilibrium is reached, the system is triphasic with a bicontinuous microemulsion in the middle phase and excess oil and aqueous phases on both sides as illustrated in Figure 1 [14][15]. We define the equilibrium state as the point where no more changes in the interfaces positions are noticed and constant properties are found in each phase with the characterization techniques used.

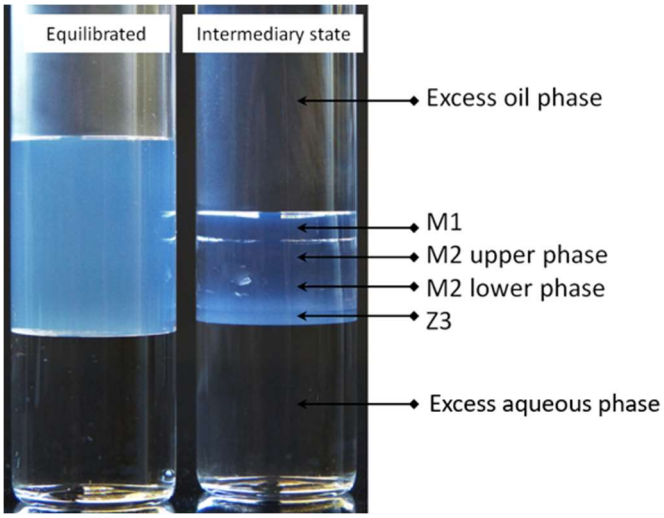

Figure 1 Photograph of the SDS/butan-1-ol/NaCl brine/toluene microemulsion at optimal formulation at equilibrium and an intermediate state

2.4. Methods

2.4.1. 1D-Composition profile from Nuclear Magnetic Resonance (NMR)

Low-Field NMR acquisitions were carried out on a 20 MHz benchtop MQR spectrometer from Oxford instruments equipped with a probe of 1.8 cm outer-diameter. The set up allows to vertically scan a tube over 2 cm in height corresponding to a 3 mL sample. The temperature was controlled at 30°C during the experiment via the injection of compressed air into the probe. For one measurement, the acquisition time is 1 min 40 s. The kinetics monitoring was stopped after 7 days of stabilization. We developed [12] a methodology that allows the simultaneous quantification of toluene, brine and butan-1-ol along the tube height. It is worth mentioning that the same method could potentially be applied to any multi-component, dark/opaque and viscous system insofar as the sample is liquid and contrasts are present between compounds. The accuracy of the method does not allow the quantification of small quantities lower than 4 % v/v in the sample. To allow data treatment, a hypothesis had to be made on SDS partition in the tube: we assumed the surfactant is entirely and homogeneously distributed in the intermediate phase(s) between excess oil and brine phases at equilibrium. This hypothesis has been verified in the literature on the same systems by carrying out Hyamine titrations or atomic adsorption tests in the excess aqueous phase and middle phase [7,11]. It is shown that 0 to 1 % w/w of surfactant remains in the excess water phase thus the surfactant is quasi-totally distributed in the middle phase. When no intermediate phase can be identified, we assumed that SDS was distributed throughout the aqueous phase. To quantify the other three compounds of the system the principle is based on 1D-imaging using weighted T1-relaxometry. Detailed information on the calculations of volume fractions from T1-relaxation profiles can be found in Supplementary Material Part II. The composition profiles resolution along the height of the tube is 100 µm.

2.4.2. Phase behavior and quantification by X-ray Micro-Computed Tomography

The X-Ray Micro-Computed Tomography (Micro-CT) tests were conducted on an EasyTom 150-160 from RX Solutions in 10 mL glass tubes of 1.8 cm-diameter at ambient temperature (~20°C). The principle is based on the transmission of X-rays radiation through the sample. In the literature, the technique is commonly used to quantify the brine from oily compounds (here, butan-1-ol and toluene) because of a strong contrast in the attenuation coefficients [6,16,17]. Practically, radiographies of the sample were acquired over time with a duration of 5 s/radiography as displayed in level of greys in Figure 5. The raw transmitted intensities were collected and corrected with an empty tube signal as refernce. The calculation of the brine volume fractions along the tube is deduced from *Equation* 1. However, no significant contrast was observed between the references [5 % w/w SDS in water] and [water]. Therefore, the presence of SDS solubilized in brine within the different phases of the microemulsion could not be detected by this technique. Moreover, the Micro-CT analysis provides precise information on the phase thicknesses and interfaces positions with a partial pixel resolution of 72 µm.

$$x_{brine}(h) = \frac{ln(I_{oil}) - ln\left(I_{sample}(h)\right)}{ln(I_{oil}) - ln(I_{brine})} \qquad \textit{Equation } 1$$

With $x_{brine}(h)$: the volume fraction of brine at height h in the sample, I_{oil} and I_{brine}: the respective transmitted intensities of separate brine reference and toluene reference (or butan-1-ol reference as the same transmitted intensities were measured for toluene and butan-1-ol).

2.4.3. Dynamic Light Scattering (DLS)

Measurements were performed using a DLS apparatus, Vasco-flex from Cordouan Technologie. The setup is equipped with a laser diode as light source (λ = 656 nm) and a single mode fiber connected to a photon counting detector. Thanks to the flexibility of the fiber, the sample was directly analyzed in its container (10 mL and 1.8 cm-diameter glass tube) so that the internal structure of the microemulsion was preserved. The diffusion measurements were conducted at an angle θ of 90° at room temperature (20°C). Data were collected and analyzed by the NanoQ software. The apparatus measures fluctuations of intensity versus time and plots the autocorrelation function *G(t)* of the scattered intensity. For random processes, the autocorrelation function is properly fitted by an exponential decay in the form written in Equation 2 If the dispersed objects are considered as spherical hard spheres having a Brownian motion,

the Stokes-Einstein relation (Equation 3) is commonly used to determine the particles size from the measurement of the characteristic relaxation time τ. In the case of a bicontinuous system or non-Brownian motion of particles, the Stokes-Einstein relation is no longer applicable and the interpretation of the relaxation times becomes more complex. In the literature, DLS studies on bicontinuous structures are scarce but one can interpret DLS relaxation times of bicontinuous microemulsions as the ability to create/break connections between oil and water domains that is to say τ is probably relative to the rate of matter exchanges through the interfacial film of oil and water domains [7,18]. Low relaxation times could be potentially linked to highly interconnected interfaces. We thus noted D_{app}, the apparent diffusion coefficient that stems from Equation 3 when referring to the bicontinuous structures or a non-Brownian motion of particles.

$$G(t) = A_0 exp(-2Dq^2t) \quad \text{and} \quad \tau = \frac{1}{2Dq^2} \qquad \textit{Equation 2}$$

With A_0 a normalization constant, τ the characteristic relaxation time of the process in µs, $q = \frac{4\pi}{\lambda} sin\ (\theta/2)$ the wave vector in m^{-1}, and D the diffusion coefficient in $m^2.s^{-1}$.

$$D = \frac{kT}{3\pi D_H \eta} \qquad \textit{Equation 3}$$

With k the Boltzman constant in $kg.m^2.s^{-2}.K^{-1}$, T the temperature in K, η the dynamic viscosity of the continuous medium in Pa.s, D_H the hydrodynamic diameter of the dispersed object in m.

2.4.4. Small Angle X-Ray Scattering (SAXS)

SAXS measurements were conducted on a Xeuss 2.0 set up from Xenocs on the Winsor III system. The microemulsions were directly formulated into quartz capillaries (diameter of 1.5 mm) to avoid sampling. We first inserted 25 µL of a pre-formulated aqueous phase using a Hamilton syringe. 23 µL of toluene was added via an iron rod above the aqueous phase to prevent any mixing in the capillary. The capillary was sealed by a drop of silicon paste. We studied two samples that were formulated in two different capillaries: a non-equilibrated system obtained 3 days after toluene addition and the equilibrated bicontinuous microemulsion measured at 7 days after toluene addition. It is worth noting that the addition speed of Toluene in capillaries cannot be controlled and implies that the equilibration times are not comparable with DLS, NMR or Micro-CT experiments even if the same processes are observed. The sample-to-detector distance was 600 mm allowing a q-range from 0.01 to 0.40 $Å^{-1}$. The X-ray beam (λ=1.54 Å) was collimated by two slits: 0.7 mm^2 and 0.4 mm^2. The calibration of the q-range was performed using standard silver behenate AgBe as reference. The intensity calibration was carried out with Lupolen only for the equilibrated sample. The cross-section intensities are given in cm^{-1} for this sample. Practically, the transmitted intensities were scanned from bottom to top in order to locate the intermediate phases. Accordingly, scattering measurements were performed at various heights. For the non-equilibrated sample, we confirmed that the system did not evolve during the experiment by carrying out another transmission scan after the experiment that overlaps the previous scan.

In the case of the bicontinuous microemulsion system, scattering was found to be isotropic and the azimuthally averaged curves I(q) were fitted using the well-known Teubner-Strey model [19,20] widely used for microemulsions SAXS data interpretation in medium q range (more information on the model can be found in Supplementary Material Part III). It gives access to the periodicity of the structure d and the correlation length ξ (i.e. the characteristic decay length of periodic order). On the SAXS curve, the position q_{max} of the characteristic peak of the microemulsions is related to $d = 2\pi/q_{max}$ and its width is related to ξ: the longer the correlation length is, the thinner the peak will be [21]. From these two parameters the amphiphilicity factor *fa* can be calculated (Equation 4). The amphiphilicity factor *fa* indicates a scale of the extent of ordering of the molecules at the interfacial film within Winsor III systems. It goes from +1 with completely disordered water/oil interfaces to -1 with well-ordered interfaces leading to lamellar phase.

$$\left(\frac{\xi}{d}\right)^2 = \frac{1}{4\pi^2}\left(\frac{1-fa}{1+fa}\right) \quad \textit{Equation 4}$$

In the case of an oriented phase [22–24], we adjusted the azimuthal profiles by a Maier-Saupe function (Equation 5) to have access to the Hermann or order parameter *S* (Equation 7) corresponding to the second moment of the normalized Maier-Saupe function (Equation 6)When *S* is equal to 1, the structure is perfectly ordered, when it is equal to 0 the structure is random. The fit also provides the angle of orientation α of the scattering objects.

$$I(\psi) = A + B\exp(m\cos^2(\psi - \alpha)) \quad \textit{Equation 5}$$

$$f_{\text{norm}}(\beta) = \frac{A + B\exp(m\cos^2(\beta))}{2\pi\int_0^{\pi}(A + B\exp(m\cos^2(\beta)))\sin(\beta)d\beta} \quad \textit{Equation 6}$$

$$S = \left\langle \frac{3\cos^2(\text{ - }\beta) - 1}{2} \right\rangle_{d\Omega = \sin\theta\, d\theta\, d\phi} = \int_0^{2\pi} d\phi \int_0^{\pi} f_{\text{norm}}(\beta)\frac{3\cos^2(\beta) - 1}{2}\sin(\beta)d\beta \quad \textit{Equation 7}$$

Where *A* and *B* are normalization constants; *m* is the orientation parameter accounting for the liquid crystal interactions; ψ is the azimuthal angle; α the orientation angle of the liquid crystals; $\beta = \psi - \alpha$.

3. Results and discussion

3.1. Equilibrium state characterization

The compositions of the final system after equilibration calculated from Micro-CT and NMR profiles are given in Table 1. A good agreement is found between the two techniques showing that the kinetics monitoring could be carried out. Micro-CT is more reliable than NMR in assessing the thicknesses of the different phases and NMR provides additional information on the co-surfactant distribution given a better contrast between butan-1-ol and water/toluene. With Micro-CT, we found that the final triphasic system is made of 36 % v/v of a bicontinuous phase, 34 % v/v of excess oil phase and 30 % v/v of excess aqueous phase.

Table 1 Composition of the equilibrated SDS/butan-1-ol/NaCl brine/Toluene microemulsion at optimal formulation – from NMR and Micro-CT

% volume	Phase	Brine + SDS	Others
Micro-CT (+/- 2 % v/v)	Excess oil	(2)	98
	Bicontinuous	48	52
	Excess aqueous	98	(2)

		Brine	SDS	butan-1-ol	Toluene
NMR (+/- 4 % v/v)	Excess oil				100
	Bicontinuous	42	5*	14	39
	Excess aqueous	97		(3)	

() Not significant
* Determined by hypothesis

3.1.1. Middle bicontinuous phase

As depicted in Figure 4 h., when equilibrium is reached, an homogenous composition of brine, butan-1-ol, SDS and toluene is found in the middle phase. NMR calculations in the middle phase lead to percentages of 47 % v/v of [brine +SDS] (48 % v/v with Micro-CT); 14 % v/v of butan-1-ol ; 39 % v/v of Toluene. The results are coherent with the data provided by Bellocq et al. [11] on the same system

for a co-surfactant/surfactant ratio of 2 at optimal salinity where 52.5 % w/w of brine and 33.5 % w/w of oil were measured in the middle phase. Similarly, for the composition, no structural gradient was found neither in SAXS nor in DLS (Figure 2). The relaxation time of the bicontinuous middle phase is about 60 µs leading to a diffusion coefficient D_{app} = 2.3x10^{-11} m²/s. In addition, the SAXS results confirmed the presence of a bicontinuous « sponge-like » structure with a characteristic peak in the intermediate q-range. A correlation length ξ of 13 nm was found and domains periodicity d is 31 nm leading to a deduced amphiphilicity factor fa of -0.75 which indicates that the microemulsion forms a distinct phase [25]. DLS and SAXS results are in agreement with the literature for similar systems at optimal salinity [7,26–29].

3.1.2. Composition in the excess oil phase

At equilibrium, no butan-1-ol is detected in the excess oil phase in the limit of detection of our method (Figure 4 h.). Also, the phase does not scatter neither in light nor in the X-ray domain (position F in Figure 7). This confirms that no dispersed object was present in the excess oil phase which is thus composed of toluene.

3.1.3. Composition in the excess aqueous phase

In the excess water phase, butan-1-ol is found at around 3 % v/v with NMR. The value is coherent with Micro-CT where 2 % v/v of other species were detected in the excess aqueous phase. However, this result is not significant regarding the respective accuracy of each method. Nevertheless, it is likely that small quantities of butanol (< 2 % w/w) could remain in the excess aqueous phase as it was previously reported on the same system [11,30]. As the excess oil phase, the aqueous phase does not scatter visible light.

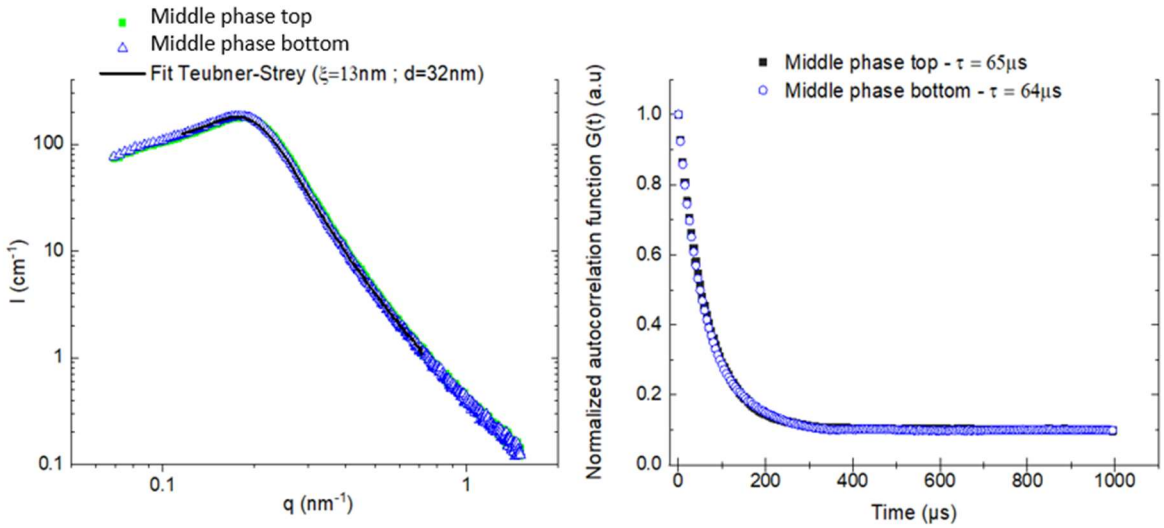

Figure 2 Characteristics of the equilibrated middle phase from SAXS and DLS measurements. Left: SAXS in absolute intensity (cm^{-1}) versus the scattering vector q (nm^{-1}) at the bottom and top in the middle phase fitted with Teubner-Strey model ; right: DLS Normalized Autocorrelation function G (a.u) in function of time (µs) at the bottom and top in the middle phase.

3.2. Kinetic study of the microemulsion formation

We illustrated in Figure 3 the different configurations of the sample that were observed in this work during the formation of the microemulsion. The process can be divided into different sections that will be commented below:

a. The initial aqueous phase
b. The oil/aqueous phase contact

c. The original formation of M2 phase
d. The evolution of the system into three intermediate phases called “Z3”, “M2” and “M1”
e. The kinetic aspects leading to the disappearance of the liquid crystal
f. The growth of the bicontinuous phase with the fading of M2 and Z3.

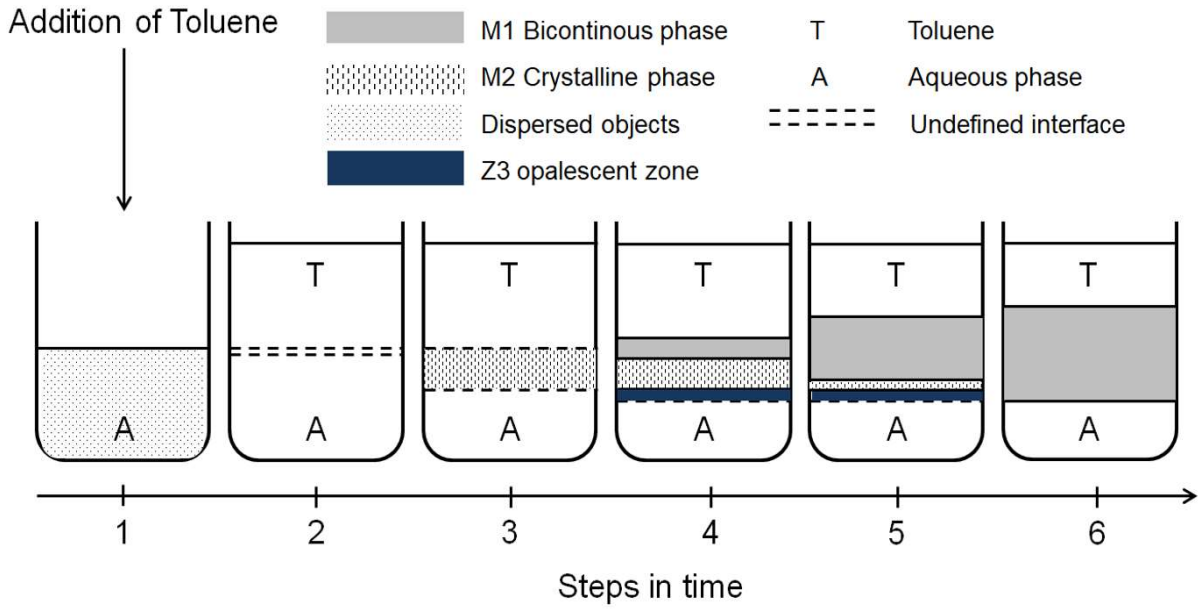

Figure 3 Schematic description of the phases behavior in the system during the formation of the microemulsion – from the Toluene addition to the equilibrium

The mechanisms described here were the same independently of the total volume of the system (~50 µL for SAXS, 3 mL for NMR and 10 mL for DLS and Micro-CT). However, the volume of the system has an impact on its equilibration time. At an oil addition speed of 126.8 mL/hour at ambient temperature, a 3 mL-microemulsion needs 7 days to stabilize while a 10 mL-microemulsion reaches equilibrium in 100 days. Kinetics results for NMR, Micro-CT and DLS are given respectively in Figure 4, Figure 5 and Figure 6. The SAXS acquisitions were performed solely at step 4 (Figure 3) when the three intermediate phases coexisted. The corresponding scattering pictures, acquired in function of height in capillaries, are displayed in Figure 7. SAXS scattering curves for each position in the capillary are shown in Figure 8.

a. Initial aqueous phase

Initially, we added 4 % w/w of SDS, and 10 % v/v of butan-1-ol in 54 g/L of NaCl brine as the aqueous phase (Figure 4 a.). Using DLS and a cumulant analysis, measurements at several values of q confirm a linear relationship between $1/\tau$ and q^2 in the aqueous phase, characteristic of a diffusive process. The average value of the observed object hydrodynamic diameter is D_H = 40 nm. An SBL-type analysis of the autocorrelation function reveals the presence of polydisperse objects with a size distribution between D_H = 20 nm and 70 nm. However, typical sizes measured for SDS spherical micelles have an hydrodynamic radius D_H of 4-6 nanometers [31]. As a result, we deduce that the initial aqueous phase at optimal salinity is not mainly made of spherical micelles. It is found in the literature that the addition of salt and alcohol to micellar solution of SDS leads to the formation of rod-like or worms micelles and even surfactant bilayers either vesicles or lamellar phases at higher concentration [32,33]. Small Angle Neutron Scattering experiments (results to be published) were performed in such phase for wave vectors q between 0.004 and 0.4 $Å^{-1}$. It confirmed the presence of cylindrical-shape micelles of 25 nm-length and 2 nm-diameter but did not exclude the presence of larger objects as our lower q-range is limited. The SANS and DLS results are compatible in the sense that the DLS scattering signal accounts for the pseudo-spheres associated with the cylindrical objects.

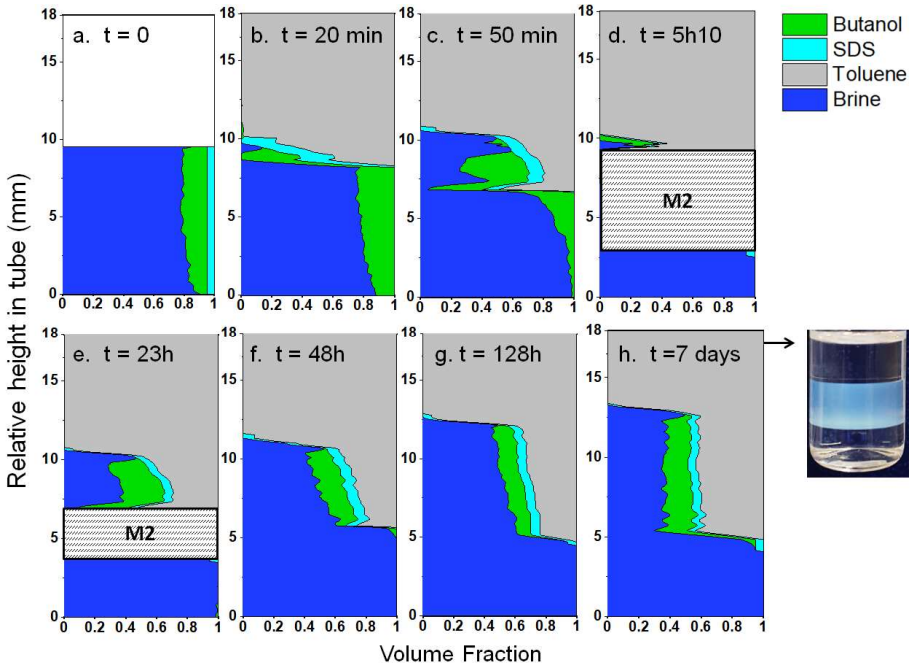

Figure 4 Composition profiles after Toluene addition onto the aqueous phase until equilibrium is reached - Total volume 3 mL– calculated from NMR 1D-relaxation profiles. The dashed zones correspond to a region where quantification is not possible due to the presence of the liquid crystal phase.

b. Oil/aqueous phase contact

After phases contact, we noticed that the butan-1-ol progressively migrated at the interface between the aqueous phase and toluene as seen in the NMR compositions profiles (Figure 4 b. and c.). This is characterized by an increase in the brine volume fraction in the aqueous phases between t = 0 to 1 day with our Micro-CT method (see Supplementary Material Part IV). As a confirmation of this effect, the bulk aqueous phase no longer scatters light one day after toluene addition. The upper oily phase also does not scatter light and still corresponds to toluene (Figure 4 b. and c.). We deduced that the surface-active species, SDS and butan-1-ol, diffused to the new interface to lower surface tensions when the two initial phases come into contact at t = 0. Visually, the system is still composed of two phases: oil and aqueous phase with an undefined and turbid interface.

c. Original formation of the M2 phase

The third step (Figure 3) is the formation of a first intermediary phase called M2 between the aqueous and oil phases. The situation is illustrated by Figure 4 d. with NMR, Figure 5 with Micro-CT and Figure 6 with DLS. The interfaces of M2 with the oil and aqueous phases are diffuse and opalescent. Macroscopically, the M2 phase is clear and birefringent by observation under crossed polarizers. Surprisingly, at the location of M2, we observed a sharp loss of NMR signal that stems from a drop in T1-relaxation times [34,35], which is displayed as the hatched area (Figure 4 d.). This is due to a drastic reduction of molecules mobility. The local structure is considered as a new species that has a specific relaxation time significantly different from the bulk case. Because this region could not be separately measured, we could not have access to the characteristic T1-relaxation time. Consequently, the complete composition could not be extracted in this zone. We were limited to the fact that M2 is made of a [brine + SDS]-rich phase up to 90 % v/v (Figure 5). Despite its birefringence, from DLS analysis, the M2 phase has a characteristic relaxation time of 71 µs which is the same at the top and bottom of M2 (Figure 6). Due to the evidences of birefringence, its NMR behavior and composition, we deduce that M2 is probably a SDS liquid crystal. Indeed, in the literature, the phase diagram of SDS/water confirms the presence of a semi-crystalline phase at a high concentration of surfactants (~ 30 % w/w) [36–38].

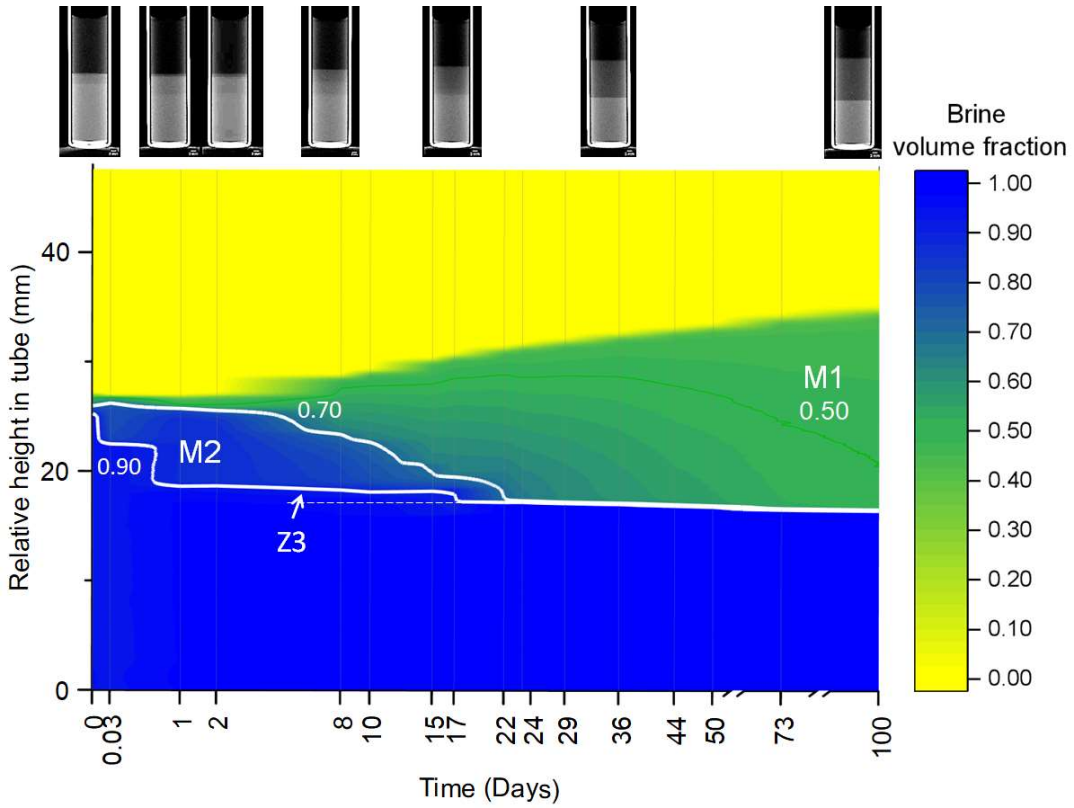

Figure 5 Brine volume fraction mapping in function of height in the tube and time (Total volume = 10 mL) - calculated by Micro-CT from the corresponding radiographies of the tube in time in level of grey, displayed above. Vertical lines show the times where the acquisitions were carried out. White lines represent the composition contours as guidelines. The dashed horizontal white line is indicative of the interface of Z3 with the excess aqueous phase as it cannot be highlighted with the chosen color map. (See in Supplementary Material Part IV that details a better representation of Z3).

d. Evolution of the system into three intermediate phases: "Z3", "M2" and "M1"

The fourth step is characterized by a more complex intermediate zone (Figure 3). The situation is related to Figure 4 e. in NMR, and between 2 to 8 days in Micro-CT (Figure 5) and DLS (Figure 6). At this stage, the liquid crystal, that was located between the excess oil and water phases, tends to form supernatant and underlying layers with well-defined interfaces. The sample is now composed of excess oil and aqueous phases, and three intermediate phases that are respectively called M1, M2 and Z3 from top to bottom.

We first analyzed the composition of such a system. The excess aqueous and oil phases are mainly composed of brine and toluene respectively. The bicontinuous phase M1 is made of toluene, SDS, brine and a high volume fraction of butan-1-ol (25 % v/v). Butan-1-ol is homogenously and entirely distributed in M1 but small gradients of oil and brine are present (Figure 5 and Figure 4 e.). Regarding M2 phase, significant gradients of composition emerged as seen on the Micro-CT colormap in Figure 5 after about 3 days. The brine volume fraction varies between 60 % v/v and 80 % v/v in M2 from top to bottom of the tube. Finally, Z3 is an homogenous phase containing 96 % v/v of brine given by Micro-CT (see detailed raw profiles in Supplementary Material Part IV).

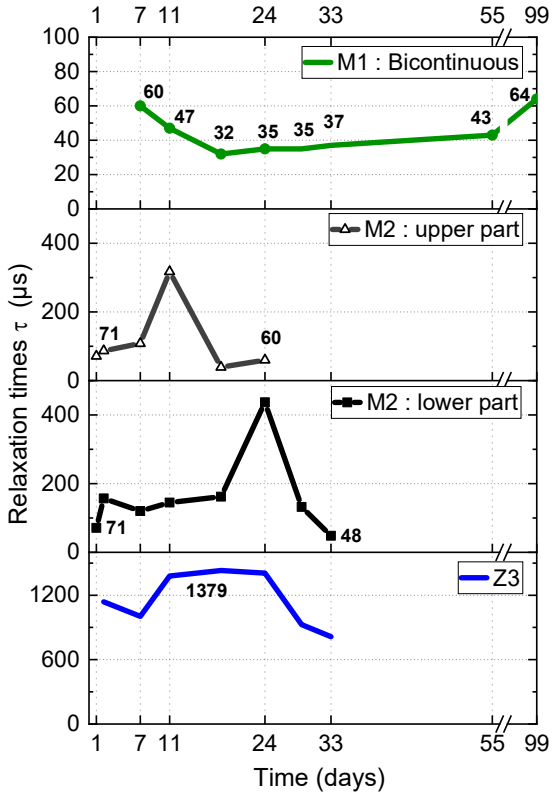

Figure 6 Evolution of relaxation times during the formation of the microemulsion in the intermediate phases from top (M1) to bottom (Z3) (Total Volume = 10 mL) – Extracted from a classical cumulant method from Dynamic Light Scattering measurements at θ= 90°- Vertical lines represent the acquired measurements times.

When analyzing the structure and dynamics of the systems, we focused on SAXS and DLS measurements at the formation of the three intermediate phases. The corresponding figures are respectively Figure 7, Figure 8 and Figure 6 at day 7. Excess oil and aqueous phases do not scatter visible light or X-Ray (position F in Figure 7) and are coherent with the found compositions. Concerning M1, we found that it has the same dynamics as the equilibrated microemulsion (Figure 6). We also confirmed that M1 is a bicontinuous microemulsion of which SAXS scattering patterns can be fitted by the Teubner-Strey model (Figure 8). A structural gradient is present in the bicontinuous phase. Indeed, the periodicity of the domains and the correlation length ξ are gradually different from the bottom to the top of the capillary passing from (d=19 nm; ξ=9.5 nm) to (d=22 nm; ξ=11 nm) respectively. We assume that these structural gradients are related to the compositional ones described above. In that sense, a higher concentration of oil would imply larger domains of the bicontinuous network. Additionally, the amphiphilicity factor fa = - 0.81 is relatively constant in M1 and smaller than the one measured at equilibrium (fa = - 0.75). The structure of the bicontinuous phase, at this time, appears to be more ordered compared to the final one. The decrease of fa in time arises from the increase in domains sizes linked to the incorporation of both water and oil in the bicontinuous phase.

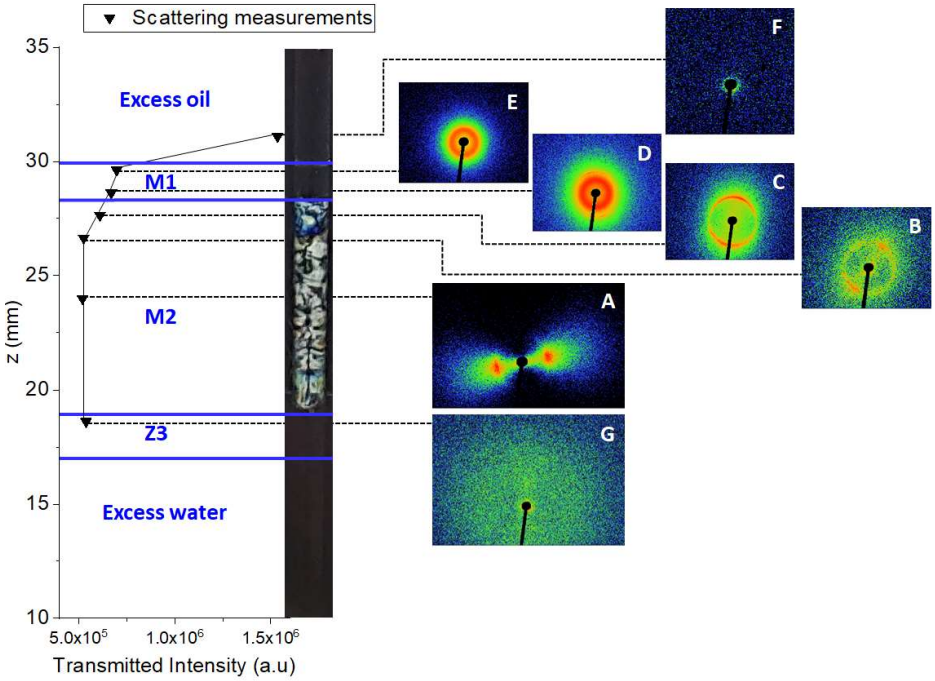

Figure 7 Schematic description of the SAXS experiment on a non-equilibrated microemulsion. (left) Location of the measured scattering points and corresponding transmissions in function of height z in the tube – (middle) Observation of the M2 phase in the SAXS capillary under crossed-polarized light. – (right) The scattering acquisitions that are represented at each measurement point in the sample.

In M2, the upper and lower parts of M2 now show distinct values of relaxation times meaning that they are significantly different in terms of dynamics and probably in structure (Figure 6). Under crossed-polarizers, the whole M2 phase is still birefringent and we could clearly identify a change in morphology along the capillary (Figure 7). Indeed, a variety of structures is found in M2 (Figure 7, Position A to C). At the center of M2 (Figure 7 at position A), the azimuthal profile $I(\psi)$corresponds to a vertically oriented liquid crystal phase with a characteristic lamella size (period) of 11 nm (Table 2). The objects have an angle of orientation of 10° and an order parameter of 0.44 (Figure 8), which is characteristic of highly ordered objects. When approaching M1, the objects preserve their sizes but progressively change their orientation (position B, C, D) by rotation until reaching a perpendicular position with an angle of orientation α of 96° (Table 2). The origin of such an orientation remains questionable, it could potentially stem from steric molecular interactions or could be influenced by the initial addition of toluene onto the aqueous phase. The parameter S that characterizes the ordering of the system, i.e. here linked to its anisotropy, decreases when passing from M2 to M1 as described in Table 2. The change in structure goes through a point (B on Figure 7) where both the bicontinuous network and the liquid crystal phase coexist in a similar proportion. At this point, the parameter S is not consistent due to a significant noise in the scattering signals. Above the interface with M2, the structure loses orientation in M1 (position D, E on Figure 7). These are direct evidences of the progressive restructuring of SDS molecules from liquid crystal (in M2) into monolayers (in M1). The sizes of the lamella in M2 are similar to the correlation length ξ of the objects in the bicontinuous phase (~ 10 nm), which is in some cases approximated as the length where the interfacial film is flat [39,40]. Consequently, it is possible that the bicontinuous network arises from the merging of the sub-units of M2. Regarding the structure type [41–43], M2 at position A and B stems from nematic phases as only one and relatively broad scattering peak is detected on the SAXS scattering plots in M2 (Figure 8 at position A, B) [22]. At position C, the peak is sharp and no second order peak is observed. Such a structure is questionable and could be either an electrostatic pseudo-lamellar phase or a smectic phase or an electrostatically swollen sponge phase [44,45] in equilibrium with the sponge phase of position D.

Table 2 Parameters extracted from the Maier-Saupe fits at position A, B, C, D in M2/M1 region introduced in Figure 7. Raw data are available in Supplementary material Part VI

Position	Order parameter S	Orientation angle α (°)	Periodicity (nm)
A	0.44	10	11
B	(0.04)	51	11
C	0.14	77	11
D	0.063	96	11

Concerning the Z3 phase, it is an opalescent and isotropic zone of relatively constant thickness located between the excess aqueous phase and M2. Z3 is hardly detectable with NMR because it is too close to M2 phase where the signals are strongly impacted by the semi-crystalline structure. In DLS, the simple cumulant inversion method leads to relatively high relaxation times in Z3 phase that are characteristic of large objects in the range of ~100 nm as seen in Figure 6. A polymodal, thus more adapted, Pade inversion analysis was carried out at different angles θ of 30; 45; 90 and 135°. It follows that the process of relaxation is diffusive and characterized by two diffusion coefficients $D \sim 5.10^{-11}$ m².s^{-1} ($D_H = 20\,nm$) and $D \sim 5.10^{-12}$ m².s^{-1} ($D_H = 200\,nm$). Because there is one decade between those two coefficients, the result is compatible either with a polydisperse distribution of objects or a bimodal distribution. Regarding the structure, the interpretation of the SAXS data in Z3 is ambiguous as we do not know its dilution regime, and because our lower q-range is limited at 0.01 Å^{-1}. However, we noted that it could be fitted using a two-population "core-shell structure with thin shell" form factor as detailed in Supplementary Material Part VII. The diameters found are 20 nm (length) and 1.4 nm (radius). DLS and SAXS agree to state that Z3 contains polydisperse core-shell structures but the observation range varied between the two techniques. Further SAXS or SANS experiments would be appreciated to characterize more precisely Z3. We assume that such a phase may appear to ensure the continuity of the thermodynamical properties between the liquid crystal and the excess brine phase.

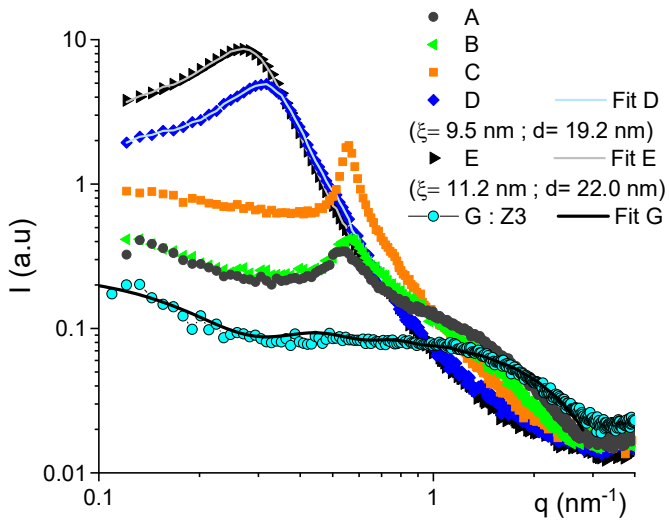

Figure 8 Scattering profiles according to the position in the capillary introduced in Figure 7. Scattering curves in M1 (D, E) were fitted by the Teubner-Strey model; Scattering curves in M2 (A, B, C, (D)) with Maier-Saupe fits. Scattering pattern for point G (divided by 5 for better representation) was fitted with a two-populations core-shell form factor (see in Supplementary Material Part VII).

The given analysis leads us to wonder why the system is structured in layers as described above. In the literature, the nucleation of different phases in the vicinity of the original interface has already been observed in various systems and explained by the differences in diffusion coefficients of the species [46][47]. In our case, the layering is caused by a competition between the migration of the surfactant and the co-surfactant towards toluene. Butan-1-ol is likely to diffuse quickly and totally to the toluene interface immediately after phases contact because of its total solubility and small molecular weight (M_w

= 74 g/mol). At the opposite, as a bigger molecule (M_w = 288 g/mol), SDS diffuses with a lower rate to the new interface (see Supplementary Material Part VIII for the reported value of self-diffusion coefficients). The difference between SDS and butan-1-ol diffusivities implies the presence of high composition gradients in the system. Thus, several assemblies of SDS are encountered in function of the height in the system as if the tridimensional phase diagram of the quaternary system was partially covered [11,48,49]. Indeed, it is known that the molecular exchanges with surfactants occur in the range of the nanosecond to the microsecond [50,51]. Thus, the structures observed in M1, M2 and Z3 can locally be considered at equilibrium and correspond to the microstructures of the phase diagram for the compositions that were determined by NMR and Micro-CT. In Figure 9, we indicate in the Toluene/butan-1-ol/6% NaCl Brine phase diagram available in literature [11] the points that correspond to t = 0 and the equilibrium as well as the probable location of M2, M1 and Z3 phases. The limit of quantification of our methods prevents us to point out a precise point of the phase diagram. Moreover, we believe that the SDS and butanol composition gradients from bottom to the top of the tube imply that the diffusion path crosses different planes of the butan-1-ol/toluene/Brine phase diagram, each plane corresponds to a specific butan-1-ol:SDS ratio. Because butan-1-ol diffuses towards the toluene supernatant phase, the butan-1-ol:SDS ratio increases from M2 to M1 phase. This conclusion is coherent with literature where "gel" regions were observed for butan-1-ol:SDS ratio lower than 2 (equals to the ratio in the final bicontinuous phase).

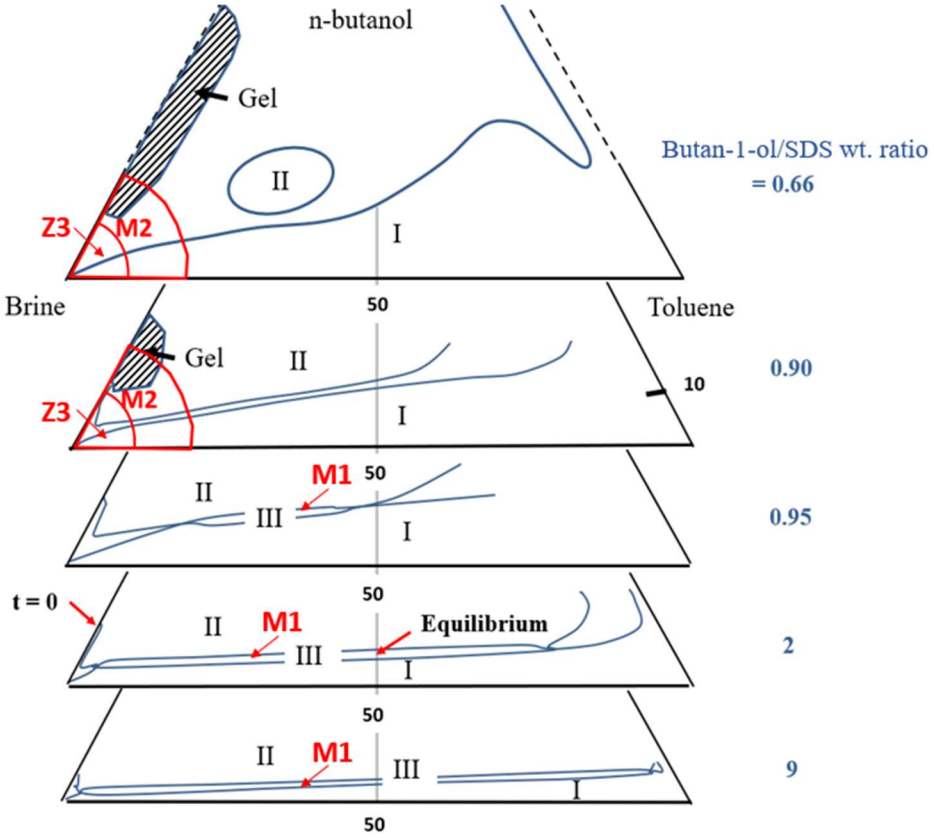

Figure 9 The ternary phase diagram n-butanol/toluene/6% NaCl brine for different planes corresponding to a specific butan-1-ol/SDS ratio [11]. In our case, n-butanol/SDS ratio is 2 at t=0 and equilibrium. The symbols I, II, III stem from Winsor I, Winsor II, Winsor III region. The dashed zone represents an identified "gel" region in literature and the red zones/arrows represent the probable locations of the M2, M1 and Z3 phases.

e. Kinetic aspects leading to the disappearance of the liquid crystal

In this part, we focused on the evolution over time of the three intermediary phases. This is related to the measurements between day 2 and day 33 in Micro-CT (Figure 5) and DLS (Figure 6). Namely, we

extracted the interfaces positions M2/M1 and M1/Oil from Micro-CT profiles and followed their behavior over time. Results are plotted in Figure 10.

Regarding the dynamics evolution of M2 over time, the upper part of M2 shows a maximum in relaxation times and then vanishes when its dynamics becomes comparable to M1 phase (Figure 6). After a few days, the lower part of M2 undergoes the same behavior. We correlate the presence of the maxima in relaxation times to the position of M1/M2 interface over time. The displacement of this maximum indicates the progressive breakage of the liquid crystal phase. Surprisingly, from Figure 10 we found that the displacement of M1/M2 interface is linear in function of time. The flux of matter exchanges through the interface from M2 to M1 is constant at a speed of 4.3×10^{-9} m.s^{-1}. Curves plots are displayed in Supplementary Material Part V for more details.

Concerning M1, its thickness increases by progressive solubilization of oil and brine by conserving a mean water/oil ratio around 50/50 v/v (Figure 5). Also, the displacement of the oil/M1 interface is proportional to $\sqrt{t}$ and thus follows Fick's law with a characteristic diffusion coefficient of 1.2 x10^{-11} m².s^{-1} as seen in Figure 10. This is in agreement with Broens et al. study in flowing conditions [5]. It means that the penetration of oil is driven by the composition gradients present in the bicontinuous phase. In addition, the DLS monitoring highlights that M1 reaches a minimum in relaxation times at the total disappearance of M2 (Figure 6). An increase of the ordering of the bicontinuous network (i.e decrease of *fa* or increase of ξ/d) could explain the decrease in relaxation times. Indeed, the correlation between ξ/d and the relaxation time τ has already been found in previous work by Fukumoto et al. [6]. In that sense, this result would particularly support the static SAXS analysis where the phase M1 was found to be more ordered than the final bicontinuous phase.

Overall, given the evidences of the dynamic and static analysis, we confirmed that the bicontinuous phase M1 is growing towards the excess aqueous interface by progressive merging with the liquid crystal M2. The liquid crystal M2 then acts like a reservoir of surfactants for the building of the bicontinuous phase M1 (i.e. the future middle phase of the equilibrated system).

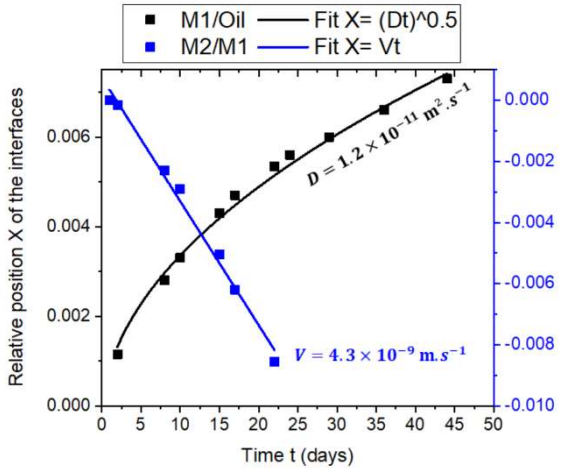

Figure 10 Relative position X of M2/M1 and M1/Oil interfaces (normalized to initial position) in function of time and fits associated.

f. The growth of the final bicontinuous phase

In the last step of the process (Figure 3), the growth of M1 finally leads to the total consumption of the liquid crystal M2. The disappearance of the liquid crystal M2 causes the inherent fading of the Z3 phase (Figure 5). This provides another source of surfactants to the bicontinuous phase M1. As a consequence, it enables the additional solubilization of toluene and water that leads to a thickening of the middle phase until equilibrium is reached (Figure 4. f., g., h. and from day 29 in Figure 5). We noticed a symmetrical growth of the middle phase along the tube leading to a centered middle phase in the final system as

expected for a microemulsion at optimal salinity [52]. Structural and compositional properties of the final system were previously commented in 3.1.

4. Conclusions

Applied to Enhanced Oil Recovery, previous kinetic studies on microemulsion formation were performed in dynamic conditions to better understand the phases behaviors of such systems in flowing conditions [4–6,53–56], especially at the vicinity of dead-end pores. However, the information extracted by such an investigation is limited due to complexity of model rocks or non-applicability of quantitative advanced techniques. To extend the knowledge on the in-situ mechanisms, we monitored in bulk the formation of a bicontinuous microemulsion from oil/water contact to equilibrium. We succeeded in using DLS, Micro-CT, NMR [12] and SAXS techniques in a non-destructive way to quantitatively analyze the properties of the system over time. First, the techniques were implemented on an equilibrated sample to assess the methods and to have access to the structure and compositions of the final system. A good agreement was found with the literature on a similar system [11,26,27,30] which made it possible to carry out the kinetic study. The work shows that the formation of the model microemulsion involves the presence of transitional layers in which structures/dynamics properties and compositions are correlated according to the position in the phase diagram [11]. We were able to identify different steps of the microemulsion formation. The initial aqueous phase contains cylindrical objects that migrate at the interface when in contact with oil. Then, an intermediate liquid crystal appears and causes the formation of the supernatant and underlying layers, respectively a bicontinuous phase and a dispersed phase. The final bicontinuous phase of the Winsor III system stems from the dismantling of the liquid crystal phase. The latter acts as a reservoir of surfactants by providing a constant matter flow toward the bicontinuous phase until total consumption. The sub-units of the liquid crystal are about 10 nm and can be compared to bricks that build up the bicontinuous network. Several types of liquid crystals that have different orientation angles were observed and should be studied in a more detailed SAXS analysis. Toward the excess oil phase, the penetration front [bicontinuous phase/excess oil] follows the Fick's law with a diffusion coefficient that is comparable to those observed under flow conditions in dead-end pores [5]. Toward the water excess phase, the liquid crystal coexits with a dispersed phase that potentially contains large vesicles. Rheological studies would be appreciated to assess the viscosity and interfacial properties of the found liquid crystal phase - provided that the liquid crystal structure is preserved when sampled. Applied to Enhanced Oil Recovery, this would give further information on the flowing behavior of such a phase in-situ in the reservoir. Indeed, the formation of a liquid crystal could potentially lead to a reservoir plugging and a decrease in oil solubilization performances at larger scale. Also, this study should provide interesting routes to understand further the mechanisms of formation of a Winsor I or II system where spherical structures are found at equilibrium. One can wonder if they also arise from a crystalline phase. It could eventually also be extended to non-ionic surfactants, i.e. when no co-surfactant is added to the formulation, to stress their roles in the mechanism of formation and have a better insight on the nature of phase transitions occurring in-situ.

References

[1] Schulman J.H., Stoeckenius W., Prince L.M, Mechanism of Formation and Structure of Micro Emulsions by Electron Microscopy, J. Phys. Chem. 63 (1959) 1677–1680.

[2] Mittal K.L., Kumar P. (Eds.), Handbook of microemulsion science and technology, Marcel Dekker, New York, 1999.

[3] Danielsson I., Lindman B., The definition of microemulsion, Colloids and Surfaces 3 (1981) 391–392.

[4] Unsal E., Broens M., Armstrong R. T., Pore Scale Dynamics of Microemulsion Formation, Langmuir the ACS journal of surfaces and colloids 32 (2016) 7096–7108.

[5] Broens M., Unsal E., Emulsification kinetics during quasi-miscible flow in dead-end pores, Advances in Water Resources 113 (2018) 13–22.

[6] Unsal E., Rücker M., Berg S., Bartels W. B., Bonnin A., Imaging of compositional gradients during in situ emulsification using X-ray micro-tomography, Journal of colloid and interface science 550 (2019) 159–169.
[7] Fukumoto A., Dalmazzone C., Frot D., Barré L., Noïk C, Investigation on Physical Properties and Morphologies of Microemulsions formed with Sodium dodecylbenzenesulfonate, Isobutanol, Brine, and Decane, Using Several Experimental Techniques, Energy Fuels 30 (2016) 4690–4698.
[8] Chen S.-H., Rajagopalan R. (Eds.), Micellar Solutions and Microemulsions: Structure, Dynamics, and Statistical Thermodynamics, Springer International Publishing, Cham, 1990.
[9] Huie L., Zhanghui W., Jiange J., Jiankun H., Chuanqin Ding, Shuang C., Partition of n-Butanol among phases and solubilization ability of Winsor type III Microemulsions, J.Surfactants and Detergents (2016), 2016 713–724.
[10] Huie L., Pingping Z., Zhanghui W., Shuang C., Chuanqin D., Solubilization Behavior of Organic Mixtures in Optimum Winsor Type III Microemulsion Systems of Sodium dodecylsulfate, J. Surfactants and Detergents (2018), 2018 497–507.
[11] Bellocq A.M, Biais J., Clin B., Fourche G., Lalanne P., Lemanceau B., Three-Dimensional Phase Diagram of the Brine-Toluene- Butanol- Sodium dodecylsulfate System, Journal of colloid and interface science 74 (1980) 311–321.
[12] Herrera D., Chevalier T., Fleury M., Dalmazzone C., Quantification of microemulsion systems using low-field T1-weighted imaging, Journal of Magnetic Resonance Imaging 83 (2021) 160-168.
[13] Salager J-L., Marquez N., Graciaa A., Lachaise J., Partitioning of Ethoxylated Octylphenol Surfactants in Microemulsion−Oil−Water Systems: Influence of Temperature and Relation between Partitioning Coefficient and Physicochemical Formulation, Langmuir 16 (2000) 5534–5539.
[14] Winsor P.A, Hydrotropy, solubilisation and related emulsification processes, Trans. Faraday Soc. 44 (1948) 376–398.
[15] Duvail M., Dufrêche J-F., Arleth L., Zemb T, Mesoscopic modelling of frustration in microemulsions, Physical chemistry chemical physics 15 (2013) 7133–7141.
[16] Scheffer K., Méheust Y., Carvalho M. S., Marcos M. H. P., Paciornik S., Enhancement of oil recovery by emulsion injection: A pore scale analysis from X-ray micro-tomography measurements, Journal of Petroleum Science and Engineering 198 (2021) 108–134.
[17] Maire E., Withers P. J., Quantitative X-ray tomography, International Materials Reviews 59 (2014) 1–43.
[18] Sharma V. K., Hayes D. G., Gupta S., Urban V. S., O'Neill H. M., Pingali S. V., Ohl M., Mamontov E, Incorporation of Melittin Enhances Interfacial Fluidity of Bicontinuous Microemulsions, J. Phys. Chem. C 123 (2019) 11197–11206.
[19] Teubner M., Strey R, Origin of the scattering peak in microemulsions, The Journal of Chemical Physics 87 (1987) 3195–3200.
[20] Breßler I., Kohlbrecher J., Thünemann A., SASfit, Journal of applied crystallography 48 (2015) 1587–1598.
[21] Oberdisse J., Hellweg T., Structure, interfacial film properties, and thermal fluctuations of microemulsions as seen by scattering experiments, Advances in Colloid and Interface Science 247 (2017) 354–362.
[22] Davidson P., Petermann D., Levelut A. M., The measurement of the Nematic Order Parameter by X-ray Scattering Reconsidered, J. Phys. II France 5 (1995) 113–131.
[23] Maier W. and Saupe A., Eine einfache molekular-statistische Theorie der nematischen kristallinflüssigen Phase., Z Naturforsch 14a (1959) 882–889.

[24] Luckhurst Gr., Zannoni C., Why is the Maier-Saupe theory of nematic liquid crystals so successful?, Nature 267 (1977) 412–414.
[25] Schubert K.-V., Strey R., Kline S. R., Kaler E. W., Small angle neutron scattering near Lifshitz lines: Transition from weakly structured mixtures to microemulsions, J. Chem. Phys. 101 (1994) 5343.
[26] Pouchelon A., Meunier J., Langevin D., Cazabat A.M, Light scattering from oil-water interfaces, J. Phyique Lett. 41 (1980) 239–242.
[27] Auvray L., Cotton J.-P., Ober R., Taupin C, Concentrated Winsor microemulsions, J. Phys. France 45 (1984) 913–928.
[28] Hayes D.G., Pingali S.V., O'Neill H.M., Urban V.S., Ye R, Observation of a structural gradient in Winsor-III microemulsion systems, Soft matter 14 (2018) 5270–5276.
[29] Engelskirchen S., Elsner N., Sottmann T., Strey R., Triacylglycerol microemulsions stabilized by alkyl ethoxylate surfactants—A basic study Phase behavior, interfacial tension and microstructure, Journal of colloid and interface science 312 (2007) 114–121.
[30] Pouchelon A., Chatenay D., Meunier J., Langevin D., Origin of low interfacial tensions in systems involving microemulsion phases, Journal of colloid and interface science 82 (1981) 418–422.
[31] Corti M., Degiorgio V., Quasi-elastic light scattering study of intermicellar interactions in aqueous sodium dodecyl sulfate solutions, The Journal of Physical Chemistry 85 (1981) 711–717.
[32] Oberdisse J., Formation spontanée de vésicules dans un système amphiphile chargé: Spontaneous formation of vesicles in a charged amphiphilic system. PhD, Montpellier II College, 2004.
[33] Méndez-Bermúdez Jose G., Dominguez H., Structural changes of a sodium dodecyl sulfate (SDS) micelle induced by alcohol molecules, Journal of molecular modeling 22 (2016) 1-9.
[34] Besghini D., Mauri M., Simonutti R., Time Domain NMR in Polymer Science, Applied Sciences 9 (2019) 1801–1834.
[35] Gradišek A., Cifelli M., Wojcik M., Apih T., Dvinskikh S., Gorecka E., Domenici V., Study of Liquid Crystals Showing Two Isotropic Phases by 1H NMR Diffusometry and 1H NMR Relaxometry, Crystals 9 (2019) 1–16.
[36] Ekwall P., Composition, Properties and Structures of Liquid Crystalline Phases in Systems of Amphiphilic Compounds, Advances in Liquid Crystals 1 (1975) 1–142.
[37] Muzzalupo R., Ranieri G.A., Terenzi M., La Mesa C., Phase Diagram and Dynamic Properties of the Ternary System Water – Sodium dodecylsulfate – Aerosol OT, Ber. Bunsenges. Phys. Chem 99 (1995) 617–623.
[38] Kékicheff P., Cabane B., Between cylinders and bilayers, J. Phys. France 48 (1987) 1571–1583.
[39] Guest D., Auvray L., Langevin D., Persistence length measurements in middle phase microemulsions, J. Phyique Lett. 46 (1985) 1055–1063.
[40] Pieruschka P., Marcelja S., Statistical mechanics of random bicontinous phases, J. Phys. II France 2 (1992) 235–2347.
[41] Holmes M. C., Charvolin J., Smectic-nematic transition in a lyotropic liquid crystal, J. Phys. Chem. 88 (1984) 810–818.
[42] Hendrikx V., Charvolin J., Rawiso M., Liebert L., Holmes M. C., Anisotropic aggregates of amphiphilic molecules in lyotropic nematic phases, J. Phys. Chem. 87 (1983) 3991–3999.
[43] Hendrikx Y., Charvolin J., Structural relations between lyotropic phases in the vicinity of the nematic phases, J. Phys. France 42 (1981) 1427–1440.
[44] Davidson P., Penisson C., Constantin D., P. Gabriel J-C., Isotropic, nematic, and lamellar phases in colloidal suspensions of nanosheets, Proceedings of the National Academy of Sciences of the United States of America 115 (2018) 6662–6667.

[45] Jho Y.S., Kim M.W., Safran S.A., Pincus P.A., Lamellar phase coexistence induced by electrostatic interactions, Eur. Phys. J E Soft Matter 31 (2010) 207–214.
[46] Laughlin R. G., The aqueous phase behavior of surfactants, Academic Press, 1994.
[47] Ricoul F., Dubois M., Belloni L., Zemb T., Phase Equilibria and Equation of State of a Mixed Cationic Surfactant-Glycolipid Lamellar System, Langmuir 14 (1998) 2645–2655.
[48] Kékicheff P., Grabielle-Madelmont C., Ollivon M., Phase Diagram of Sodium dodecylsulfate-Water System, Journal of colloid and interface science 131 (1988) 112–132.
[49] Rong G., Tianqing L., Structure Properties for SDS/ n-C4H9OH/H20 Microemulsion, Journal of Dispersion Science and Technology 20 (1999) 1327–1344.
[50] Aniansson E. A. G., Wall S. N., Kinetics of step-wise micelle association, J. Phys. Chem. 78 (1974).
[51] Aniansson E. A. G., Wall S. N., Almgren M., Hoffmann H., Kielmann I., Ulbricht W., Zana R. et al., Theory of the kinetics of micellar equilibria and quantitative interpretation of chemical relaxation studies of micellar solutions of ionic surfactants, J. Phys. Chem. 80 (1976) 905.
[52] Huh C., Interfacial tensions and solubilizing ability of a microemulsion phase that coexists with oil and brine, Journal of colloid and interface science 71 (1979) 408–426.
[53] Tagavifar M., Xu K., Jang Sung Hyun, Balhoff M. T., Pope G. A., Spontaneous and Flow-Driven Interfacial Phase Change, Langmuir the ACS journal of surfaces and colloids 33 (2017) 13077–13086.
[54] Shahidzadeh N., Bonn D., Aguerre-Chariol O., Meunier J., Spontaneous emulsification relation to microemulsion phase behaviour, Colloids and Surfaces A: Physicochemical and Engineering Aspects 147 (1999) 375–380.
[55] Alzahid Y. A., Mostaghimi P., Walsh S. D.C., Armstrong R. T., Flow regimes during surfactant flooding, Fuel 236 (2019) 851–860.
[56] Yu F., Jiang H., Fan Z., Xu F., Su H., Li J., Formation and Flow Behaviors of in Situ Emulsions in Heavy Oil Reservoirs, Energy Fuels 33 (2019) 5961–5970.